Physical Chemistry

A DFT study of ethylene polymerization by zirconocene catalysts. 1. Model system $[Cp_2ZrEt]^+ + C_2H_4$

I. E. Nifant'ev, L. Yu. Ustynyuk, and D. N. Laikov*

Department of Chemistry, M. V. Lomonosov Moscow State University, Leninskie Gory, 119899 Moscow, Russian Federation.
Fax: +7 (095) 939 4523. E-mail: inif@org.chem.msu.su

A DFT study of ethylene polymerization by zirconocene catalysts was carried out. Stationary points corresponding to intermediates and transition states were located on the potential energy surface of the $[Cp_2ZrC_2H_5]^+ + C_2H_4$ model system. Three possible reaction mechanisms involving the formation of β-agostic complexes were considered. The energy and thermodynamic characteristics for different reaction pathways were calculated. Corresponding activation energies lie in the range 3.9—6.8 kcal mol^{-1}.

Key words: ethylene, polymerization, zirconocenes, nonempirical quantum-chemical calculations, density functional theory.

Research into the mechanisms of polymerization of terminal olefins by zirconocene catalysts is a rapidly developing area of homogeneous catalysis. To date, a considerable body of experimental data has been accumulated and all prerequisites to a detailed theoretical study of this process have been reached.[1—3]

Quantum-chemical modeling of the species formed during the polymerization by zirconocene catalysts makes it possible not only to verify the assumptions based on the results of kinetic experiments, but also to obtain additional information on the details of the polymerization mechanism. Nonempirical quantum-chemical studies of metallocene molecules have long been hampered by the fact that corresponding calculations are time-consuming. However, the development of both hardware and software has sparked the interest of investigators in this investigation line. The informativeness of the results obtained by nonempirical quantum-chemical methods depends on the level of theory at which the studies are carried out and on how adequately the model under consideration fits the real catalytic system.

Currently, it is commonly accepted that polymerization of terminal olefins is catalyzed by a species (an ionic pair **1**) comprising a bis(cyclopentadienyl)alkylzirconium cation (hereafter, the alkylzirconocene cation; by alkyl is meant the growing polymer chain) and a weak nucleophilic anion A^-:

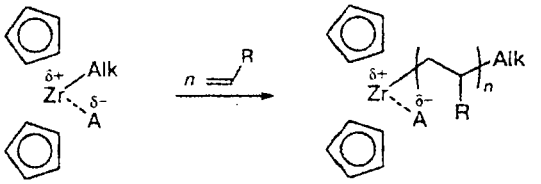

1

Usually, an active catalytic species of type **1** is generated either in the reaction of zirconocene dichloride with a large excess of methylalumoxane (in this case, the A^- anion is an alumoxane globule with the stoichiometric composition $(AlOMe)_n$ and unknown

Published in *Izvestiya Akademii Nauk. Seriya Khimicheskaya*, No. 7, pp. 1168—1177, July, 2000.

1066-5285/00/4907-1164 $25.00

structure) or in the reaction of dimethylzirconocene with tris(pentafluorophenyl)boron (in this case, $A^- = [Me-B(C_6F_5)_3]^-$).

Since anion A^- is a weak nucleophile due to both electronic and steric factors, the zirconocene species can react with olefins, thus promoting eventual their polymerization. Because of this, only the interaction between the "naked" alkylzirconocene cation and the olefin molecule is usually analyzed when considering a polymerization process. Most often, the growing polymer chain is represented by the ethyl group (Alk = Et) and the analysis is restricted to consideration of polymerization of the simplest olefin, ethylene (R = H). On the one hand, this makes it possible to reveal essential features typical of polymerization of all olefins and, on the other hand, to reduce the dimensionality of the problem and the number of structures to be calculated.

Currently, there are two approaches used in theoretical studies of metallocene catalysts and corresponding processes. The first of them is based on the classical Hartree—Fock scheme. It has been shown[4] that good agreement between calculated and experimental data can only be achieved by introducing correlation corrections at the MP2 or MP4 level of theory, which increases dramatically the computational cost. Thus, the first approach requires powerful computational resources. The second approach, which is currently receiving increasingly wider acceptance, is based on the density functional theory (DFT). Being applied to rather large molecules such as those of organometallic compounds including metallocenes (tens of atoms, 1000 basis functions and more), this approach has the advantage over other semiempirical and nonempirical methods that it allows obtaining good agreement between calculated and experimental data at a relatively low computational cost.[5]

A series of theoretical studies[6—10] by T. Ziegler and co-authors has made a great stride toward understanding the mechanisms of the processes proceeding in the polymerization of olefins in homogeneous catalytic systems. Using the DFT approach, the key stages of polymerization were revealed and realistic numerical estimates of thermodynamic characteristics of the process were obtained. An attempt has also been undertaken at

Scheme 1

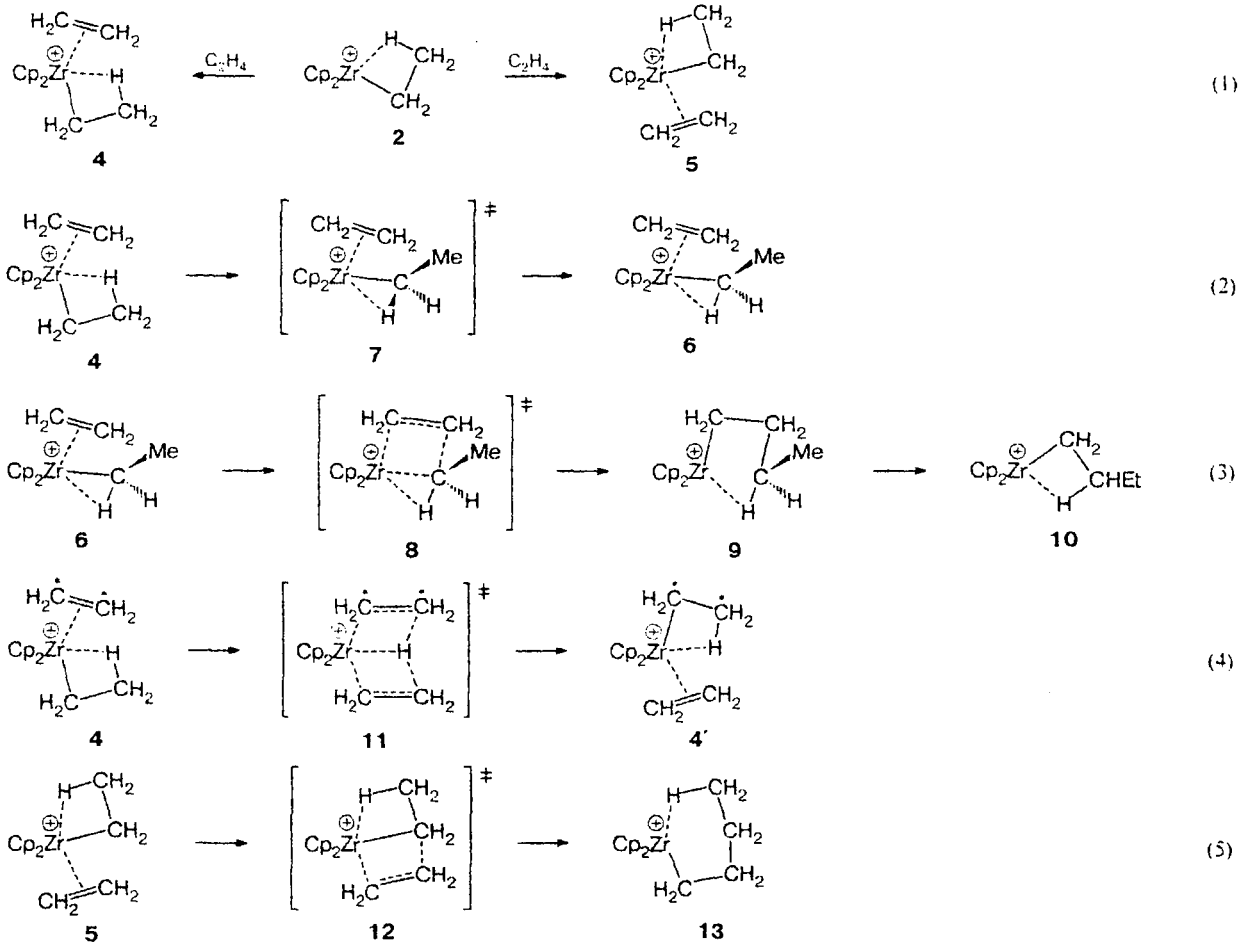

constructing a *comprehensive* model for the polymerization of olefins, in which not only zirconocene cations, but also complexes of transition metals in the d^0 electron configuration are considered as catalysts. These studies have shown that agostic interactions (hereafter, by agostic bonds are meant short metal—hydrogen intramolecular contacts which are shorter than the sum of the van der Waals radii of the corresponding atoms[11]) play an important role in these processes.

Let us briefly outline some general conclusions about ethylene polymerization by ethylzirconocene cations as model catalysts[8]:

1. The ethylzirconocene cation exists mainly as the β-agostic complex **2** with an agostic bond between the Zr atom and the β-hydrogen atom of the alkyl chain. α-Agostic compound **3** and nonagostic complexes have much higher energies.

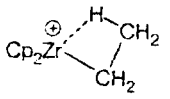

2

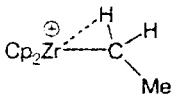

3

2. The reaction of ethylzirconocene cation **2** with an ethylene molecule can result in two types of adducts, namely, a frontside adduct **4** and a backside adduct **5** (Scheme 1, Eq. (1)). Both ethylene complexes are formed exothermically.

3. The frontside β-agostic ethylene complex **4** can undergo rearrangement into α-agostic complex **6** by rotating the ethyl fragment about the $Zr—C_\alpha$ bond by ~60° through *the only* transition state (TS) **7** (see Scheme 1, Eq. (2)).

4. A new C—C bond is formed as a result of an intramolecular process in α-agostic complex **6** through the four-center TS **8**, involving the formation of γ-agostic cation **9**, which can undergo exothermic rearrangement into the more stable β-agostic complex **10** (see Scheme 1, Eq. (3)). According to calculations,[10] the activation barrier to insertion is very low and the ethylene insertion is not the rate-limiting stage of the process. Therefore, it is the **4** → **6** rearrangement through TS **7** that controls the rate of chain propagation.

5. Chain termination occurs as a result of hydrogen transfer in the frontside ethylene complex **4** through TS **11**, involving the formation of a terminal double bond in the growing polymer chain (see Scheme 1, Eq. 4).

6. "Direct" ethylene insertion into complex **5** to give the δ-agostic complex **13** is also a feasible reaction channel (see Scheme 1, Eq. (5)). The reaction proceeds *via* TS **12**, whose energy is appreciably higher than that of TS **7**. Because of this, the activation energy of "direct" ethylene insertion is high and the corresponding reaction channel plays an insignificant role in the polymerization.

However, there are reasons to believe that the reported data on polymerization by zirconocene catalysts[8] are not exhaustive.

First, numerical estimates[8] of the energy and other thermodynamic characteristics are rather inaccurate. For instance, the free activation energy ($\Delta G^{\neq}$) for chain propagation (0.08 kcal mol^{-1} at 298.15 K) was strongly underestimated (see the original study). This is first of all due to the use of relatively small basis sets and to the absence of a self-consistent procedure for inclusion of gradient corrections to the exchange-correlation energy (for more detail, see the Calculation Procedure section).

Second, the role of the most energetically favorable adduct **5** formed in the reaction of cation **2** with an ethylene molecule is not clearly understood as yet. At the same time, both the formation of adduct **5** and its transformations, including those resulting in polymerization products, cannot be ignored. However, of all feasible transformations only selected reactions have been considered to date; therefore, the set of theoretically studied intermediates and transition states is incomplete.

At the same time, the reported qualitative data[8] on the geometry of intermediates and transition states of the reaction can be used for more in-depth studies of this process.

In this work, we present the results of our study carried out in order to gain deeper insight into the geometry and energetics of intermediates and transition states of the reaction between the model catalytic species $[Cp_2ZrC_2H_5]^+$ and the ethylene molecule, as well as of transition states of their interconversions. We found that the use of the PBE density functional and extended basis sets provides better agreement with experimental data (*cf.* Ref. 8).

Calculation Procedure

Calculations were performed using an original program which uses Gaussian basis sets for solving the Kohn—Sham equations and the electron density expansion in an auxiliary basis set for calculating the Coulomb and exchange-correlation energy.[12] The latter procedure permits improving the performance of the computational scheme by about an order of magnitude without loss of accuracy.

We used the PBE density functional[13] and contracted sets of Gaussian-type functions of size (uncontracted/contracted) (5s1p)/[3s1p] for H atoms, (11s6p2d)/[6s3p2d] for C atoms, (15s11p2d)/[10s7p2d] for Si atoms, and (21s16p12d)/[15s12p7d] for Zr atom. The auxiliary basis sets were uncontracted sets of Gaussian-type functions of dimension (5s1p) for H atoms, (10s3p3d1f) for C atoms, and (21s9p9d8f8g) for Zr atom.

Molecular geometries were optimized without imposing symmetry restrictions. The types of stationary points located on the potential energy surface (PES) were determined from analytical calculations of the second energy derivatives and vibrational frequencies.

Table 1. Comparison of calculated and experimental geometric parameters for $H_2SiCp_2ZrCl_2$ (**14a**) and $Me_2SiCp_2ZrCl_2$ (**14b**)

Parameter	Calculation[a]	Data of X-ray study[a]	This work	
	14a	**14b**	**14a**	**14b**
Distance/Å				
Si—C (Cp)	1.90	1.88	1.88	1.89
Zr—Cp(center)	2.26	2.23	2.25	2.24
Zr—Cl	2.49	2.43	2.45	2.45
Angle/deg				
Cp(center)—Zr—Cp(center)	131.8	126	125.5	125.5
Cl—Zr—Cl	105.2	98.6	102.4	102.4

[a] Data taken from Ref. 9.

Results and Discussion

Comparison of calculated and experimental geometries of model compounds $R_2SiCp_2ZrCl_2$ (R = H, Me)

Agreement between calculated and experimental geometric parameters of bis(cyclopentadienyl)zirconium complexes can be shown taking Si-bridged bis(cyclopentadienyl) *ansa*-zirconocene dichlorides **14a,b** as examples (Table 1). The structure of *ansa*-zirconocene **14a** was calculated previously.[9] In Table 1, these data are compared with the results of X-ray study of compound **14b**. The results of our calculation of molecules **14a** and **14b** are also presented in Table 1.

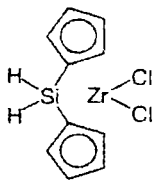

14a

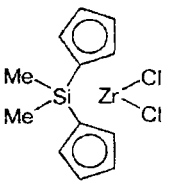

14b

The data listed in Table 1 indicate that the computational method employed in this work adequately reproduces the geometries of the systems under study. It should be noted that the calculations of compounds **14a,b** performed using the PBE functional reproduce the geometry of metallocenes better than the calculations reported earlier.[8,9]

In addition to the size of the basis set, the computational method we used has another important feature. In this work, the geometry optimization was performed using the self-consistent procedure for the inclusion of gradient corrections. Previously,[8,9] this was done with the Vosko local exchange-correlation potential[14] and a non-self-consistent procedure for introducing gradient corrections using the Becke exchange functional[15] and the Perdew correlation functional.[16,17] This could also be the reason why our data are in better agreement with experiment (see Table 1).

Structures and energies of initial compounds and primary reaction products

The optimized structure of initial complex $[Cp_2ZrC_2H_5]^+$ (**2**) is shown in Fig. 1 and the geometric parameters of the complex are listed in Table 2. The agostic bond between the Zr atom and the β-H atom of the ethyl group is the key feature of this structure. The Zr—H(7) distance is 2.11 Å, which is less than the sum of the van der Waals radii of zirconium and hydrogen (2.5 Å). The C(2)—H(7) bond is appreciably lengthened as compared to the ordinary C—H bond in alkanes (1.17 *vs.* 1.10 Å, respectively). The H(7) atom is in the plane passing through the Zr atom and the C(1) and C(2) atoms of the ethyl group. The Zr—C(1)—C(2)—H(7) dihedral angle is only 0.1°. Structure **2** is characterized by slight deviations from C_s symmetry.

The reaction of an ethylene molecule with cation **2** results in adducts **4** and **5**.[8] The structures of complexes **4** and **5** obtained from our geometry optimizations are presented in Fig. 2, *a* and Fig. 2, *b*, respectively, and their energies and geometric characteristics are listed in Table 2. A characteristic of complexes **4** and **5** is the Zr—H(7) β-agostic bond, as is the case of initial cation **2**. The Zr—H(7) distances are 2.18 Å (**4**) and 2.12 Å (**5**) and the C(2)—H(7) bond length in both structures is 1.16 Å. Complexes **4** and **5** have asymmetric structures. First of all, this is due to the fact that the coordinated ethylene molecule is not in the plane passing through the zirconium atom and the C(1) and C(2) atoms of the ethyl group, namely, the C(1)—Zr—C(3)—C(4) dihedral angle is −9.0° (**4**) and −15.7° (**5**). It should also be noted that the Zr—C(3) and Zr—C(4) distances in the more stable complex **5** are appreciably shorter than the corresponding distances in complex **4**. This is likely due to greater steric hindrances produced in the latter case and can be responsible for the lower stability of complex **4** (see Table 2).

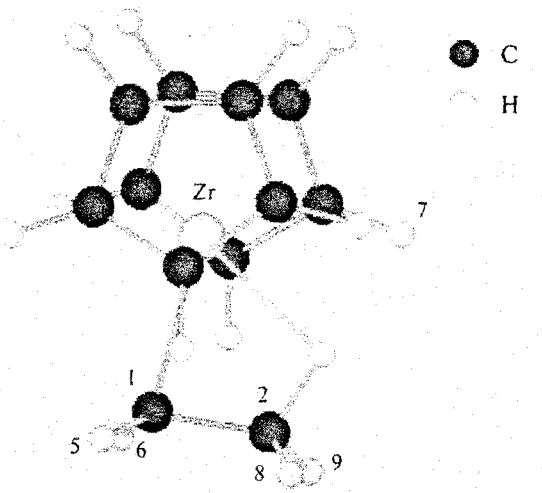

Fig. 1. Structure of complex $[Cp_2ZrC_2H_5]^+$ (**2**).

Table 2. Energies and geometric parameters of reagents ($[Cp_2ZrC_2H_5]^+$ (**2**) and C_2H_4), $[Cp_2Zr(C_2H_5)C_2H_4]^+$ complexes (**4** and **5**), transition states **7** and **7'**, and reaction product $[Cp_2ZrC_4H_9]^+$ (**9**)

Parameter	**2** + C_2H_4	**4**	**5**	**7**	**7'**	**9**
Energy[a]			*E*/kcal mol^{-1}			
	0	−11.5	−12.4	−6.3	−6.1	−23.2
Bond length[b]			*d*/Å			
Zr—C(1)	2.27	2.35	2.35	2.28	2.28	2.65
Zr—H(7)	2.11	2.18	2.12	3.63	3.69	4.56
C(1)—C(2)	1.50	1.49	1.50	1.53	1.53	1.54
C(3)—C(4)	1.33	1.35	1.36	1.35	1.35	1.56
C(1)—H(6)	1.09	1.09	1.09	1.12	1.11	1.14
C(2)—H(7)	1.17	1.16	1.16	1.10	1.10	1.10
Interatomic distance			*l*/Å			
Zr—C(3)	—	2.87	2.76	2.77	2.80	2.23
Zr—C(4)	—	2.88	2.81	2.86	2.82	2.66
Zr—H(6)	2.90	2.97	3.02	2.61	2.67	2.21
C(1)—C(4)	—	4.25	2.76	3.15	3.19	1.57
Bond angle			α/deg			
Zr—C(1)—C(2)	84.2	84.7	82.8	126.5	127.5	152.8
Zr—C(3)—C(4)	—	76.8	78.0	80.1	76.5	87.1
C(1)—Zr—C(3)	—	135.5	90.6	96.5	100.2	67.3
Zr—C(1)—H(6)	114.6	114.7	118.0	93.9	97.9	55.1
Dihedral angle			ω/deg			
C(1)—Zr—C(3)—C(4)	—	−9.0	−15.7	−37.6	−29.6	−18.4
C(3)—Zr—C(1)—C(2)	—	−1.8	1.5	−57.0	76.0	−57.7
C(3)—Zr—C(1)—H(5,6)	—	63.1	−65.2	78.5	−55.8	88.3
	−67.6	67.7	4.8	17.3	−19.9	
Zr—C(1)—C(2)—H(7,8,9)	0.1	1.3	1.7	−53.5	59.6	86.7
	−64.6	65.1	−62.6	6.1	−1.59	26.2
	64.9	−62.9	65.5	67.3	−62.4	−34.4

[a] All energies are given relative to isolated reagents **2** + C_2H_4.
[b] The numbering of the atoms is given in Figs. 1—4.

A local energy minimum corresponding to the third adduct **15** (see Fig. 2, *c*) was also located on the PES of the $[Cp_2ZrC_2H_5]^+ + C_2H_4$ system. Complex **15** is formed by frontside (from the side at which the agostic bond is situated) addition of an ethylene molecule to the ethylzirconocene cation. In this complex, the ethylene molecule is nearly perpendicular to the plane passing through the Zr, C(1), and C(2) atoms. The Zr—C(3) and Zr—C(4) distances (2.96 and 3.02 Å, respectively) are appreciably longer than the corresponding distances in adducts **4** and **5**. The Zr—H(7) agostic bond (2.25 Å) is longer, whereas the C(2)—H(7) bond (1.14 Å) is shorter than those in complexes **4** and **5**. These results indicate that the binding energies of an ethylene molecule as well as the strength of the Zr—H(7) agostic bond in adducts **4** and **5** are higher than in complex **15**, which is responsible for their higher stability. The energy of adduct **15** is 2.7 kcal mol^{-1} higher than that of complex **4**. Because of this, complex **15** seems to play an insignificant role in the polymerization reaction and is not considered below. This indicates a high mobility of the ethylene molecule in the coordination sphere of the

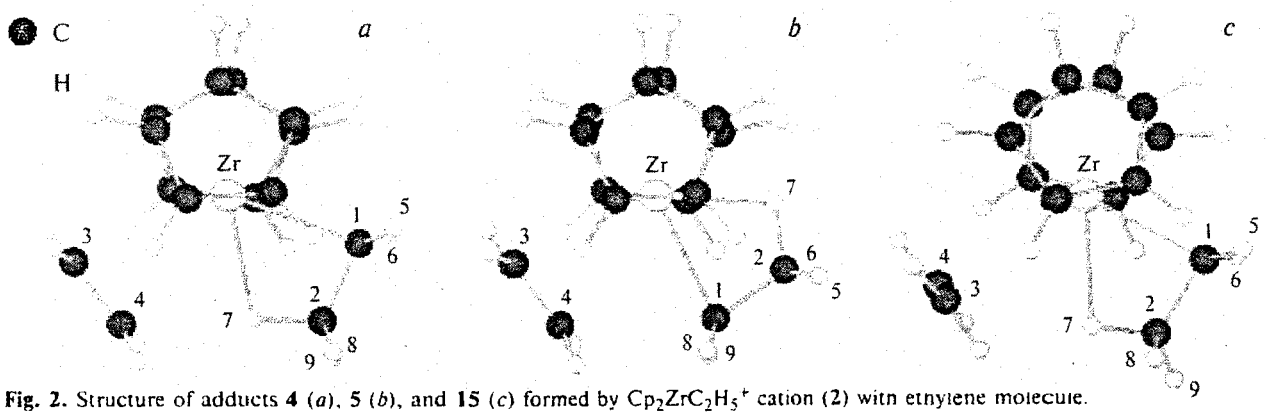

Fig. 2. Structure of adducts **4** (*a*), **5** (*b*), and **15** (*c*) formed by $Cp_2ZrC_2H_5^+$ cation (**2**) with ethylene molecule.

zirconium ion. Recently,[18] an analogous inference was made about the hydrogen molecule in related systems.

Ethylene addition and dissociation of adducts formed

Equilibrium in the 4 ⇌ 2 + C_2H_4 ⇌ 5 system

Our study of the PES of the $[Cp_2ZrC_2H_5]^+ + C_2H_4$ system showed that the ethylene molecule is added barrierlessly and that the energy of the system decreases by about 9 to 13 kcal mol^{-1} as compared to non-interacting reagents (Table 3). Though such an addition is extremely energetically favorable, it is accompanied by a substantial loss of entropy (37—45 cal mol^{-1} K^{-1}). As a result, the ΔG_{298} value for the addition reaction becomes positive. Correspondingly, the ΔG_{298} values for dissociation of adducts **4**, **5**, and **15** into molecule **2** and an ethylene molecule become negative. Hence, adducts **4**, **5**, and **15** can undergo interconversions by means of dissociation followed by addition of an ethylene molecule. If the reaction is conducted under conditions of excess ethylene, as is the case with real catalytic systems, it can be assumed that an equilibrium is established between adducts **4**, **5**, and **15** and that the equilibrium constant depends only on the difference between the free energies of the complexes. The energies and thermodynamic parameters of adducts **4**, **5**, and **15** with respect to the initial complex **2** and an ethylene molecule are listed in Table 3. The energy of complex **5** is about 0.9 kcal mol^{-1} lower than that of complex **4**. Since the Gibbs free energies (ΔG_{298}) of both complexes are nearly equal, their concentrations in the equilibrium system are also close.

Thus, studying the polymerization mechanism requires consideration of all feasible conversion pathways resulting in product **9** not only for complex **4**, as was done previously, but also for adduct **5**, which plays an important role in this system.

Energy profile of transformation 4 → 7

As was mentioned above, present views of the mechanism of polymerization by zirconocene catalysts are

Table 3. Energies and standard thermodynamic characteristics of adducts **4**, **5**, and **15** formed by complex **2** with an ethylene molecule*

Adduct	E	ΔH_0	ΔH_{298}	ΔG_{298}	ΔS_{298}
		kcal mol^{-1}			/cal mol^{-1} K^{-1}
4	−11.50	−8.91	−9.18	3.03	−41.0
5	−12.44	−9.68	−10.19	3.05	−44.4
15	−8.79	−6.32	−6.31	4.88	−37.5

* All numerical values are given relative to isolated reagents **2** + C_2H_4.

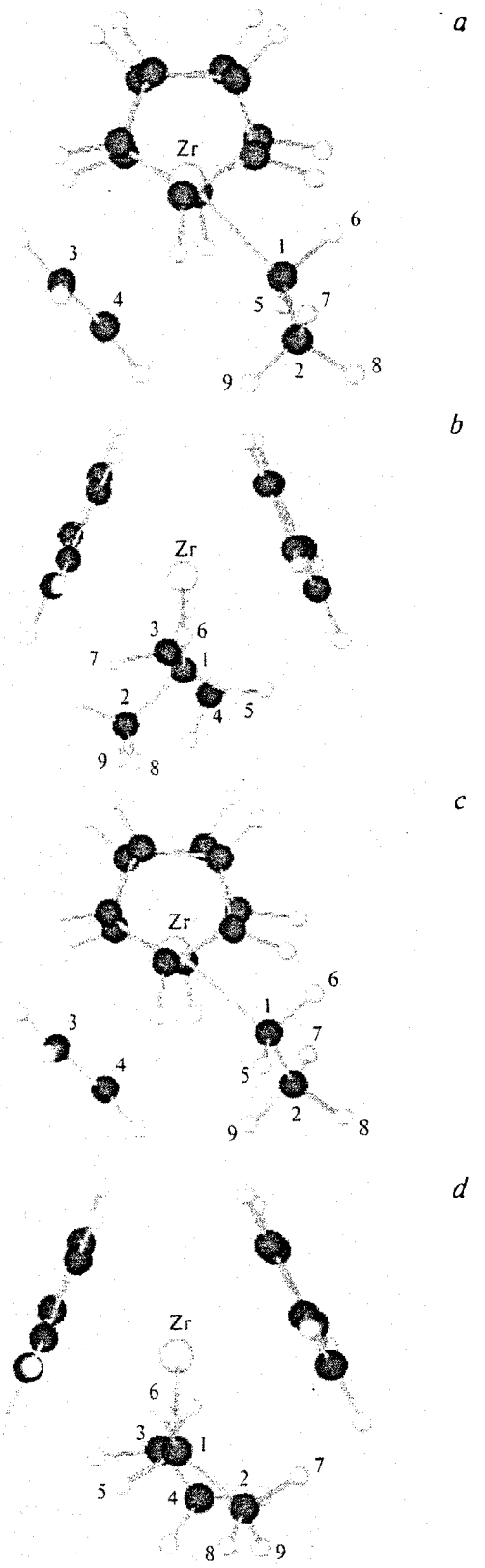

Fig. 3. Geometries of transition states **7** (*a*, *b*) and **7′** (*c*, *d*). Side views of **7** (*b*) and **7′** (*d*).

Scheme 2

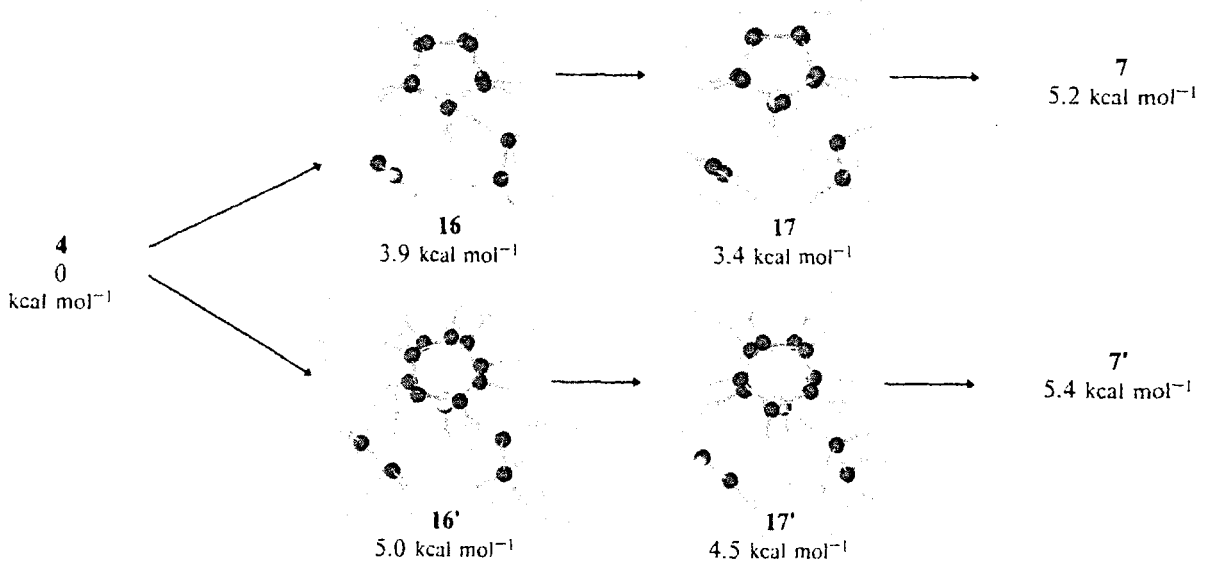

based on the hypotheses that TS **7** is reached when β-agostic complex **4** undergoes isomerization into α-agostic complex **6** and the energy of TS **7** is nearly equal to that of complex **6**. It has been shown[8] that isomerization **4** → **6** occurs by rotating the ethyl group by ~60° about the Zr—C(1) bond (see Fig. 2, *a*). Our study of the PES of the $[Cp_2ZrC_2H_5]^+ + C_2H_4$ system showed that such a rotation can occur both clockwise and counterclockwise, thus resulting in two TS, **7** and **7'**, with different geometries and nearly equal energies (5.2 and 5.4 kcal mol^{-1} relative to initial complex **4**, respectively). The geometries of TS **7** and **7'** are shown in Fig. 3. It was also found that the reaction pathway passes through a number of stationary points identified as two local maxima corresponding to structures **16** and **16'** and two minima corresponding to structures **17** and **17'** (Scheme 2). Passage through stationary point **16** (**16'**) requires overcoming of an energy barrier associated with cleavage of the C(2)—H(7) β-agostic bond (see Fig. 2, *a*).

As the angle of rotation about the Zr—C(1) bond approaches 60° (structures **17** and **17'**), the formation of the Zr—H(6) α-agostic bond begins. Structures **7** and **7'** correspond to such a situation in the system when the distortions of the geometry (first of all, a decrease in the Zr—C(1)—H(6) bond angle) are large enough, but the newly formed α-agostic bond is still insufficiently strong to compensate for the expenditures of energy due to the above-mentioned distortions. It should be noted that the possibility for two TS to exist is due to the asymmetric structure of the initial complex **4**. Previously,[8] only a symmetric structure **4** was considered; because of this, only one TS of the type **7** was found.

Realization of particular TS is determined by the direction of rotation of the ethyl group. If, *e.g.*, a clockwise rotation of this fragment about the Zr—C(1) bond leads to TS **7**, the counterclockwise rotation leads to TS **7'**.

As rotation about the Zr—C(1) bond occurs, the ethylene molecule also rotates about its center of mass in the coordination sphere of the zirconium ion and simultaneously approaches this ion and the Zr—C(3) and Zr—C(4) distances are slightly shortened (see Table 2). The ethylene molecule can rotate concurrently with or counterconcurrently to the ethyl fragment, thus resulting in TS **7** or TS **7'**, respectively.

Energy profile of transformation **5** → **7**

We also studied the mechanism of transformation of adduct **5**, which has a lower energy. This transformation also makes it possible to reach TS **7** and **7'**. As was mentioned above, complex **5** (see Fig. 2, *b*) can undergo conversion into complex **4** by means of dissociation into **2** and an ethylene molecule followed by coordination of ethylene to the other (frontside) position. There is also another chain propagation mechanism involving complex **5** (Scheme 3), namely, an intramolecular rearrangement in this complex, which leads to TS **7** or to TS **7'**. The first stage of such a transformation is the cleavage of the β-agostic bond accompanied by rotation about the C(1)—C(2) bond, which can occur both clockwise and counterclockwise. This reaction stage requires overcoming of an energy barrier associated with cleavage of the C(2)—H(7) β-agostic bond. The energies of the corresponding TS, **18** and **18'**, are 7.7 and 7.3 kcal mol^{-1}, respectively (relative to initial complex **5**), which is much higher than the energies of structures **7** and **7'**. The next stationary point on the PES is an energy minimum. The corresponding structure either has no agostic bonds (**19**) or has a weak Zr—H(5)

Scheme 3

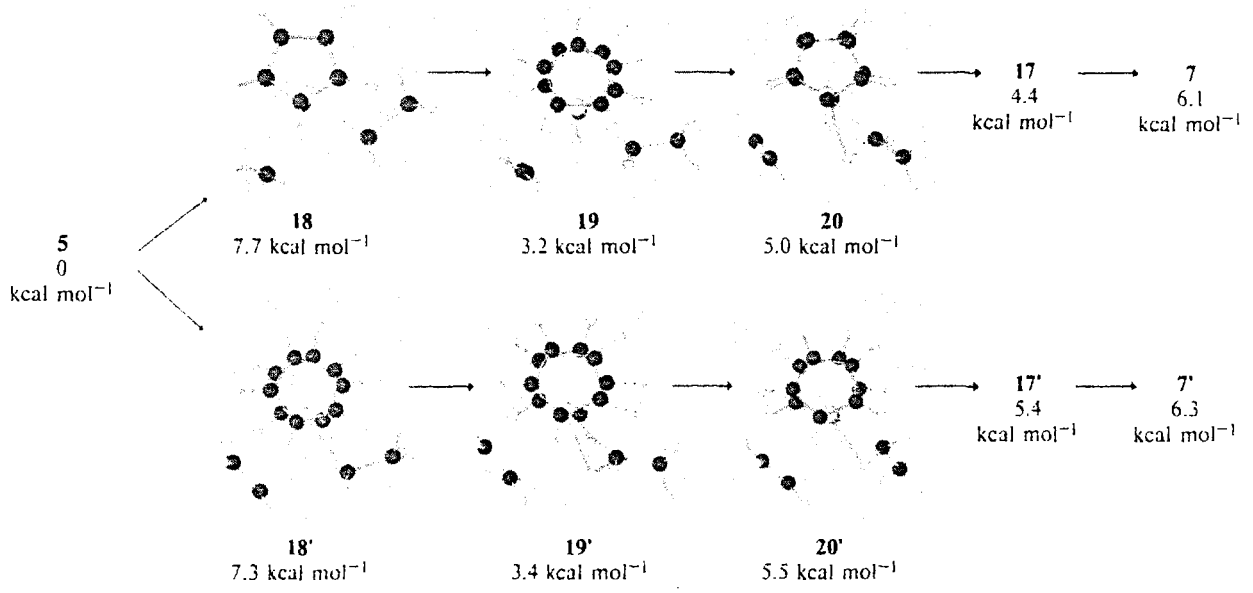

α-agostic bond (**19'**). Structures **19** and **19'** also differ in orientation of the ethylene molecule in the coordination sphere of the zirconium ion. In structure **19**, the ethylene molecule is oriented nearly perpendicular to the plane passing through the Zr, C(1), and C(2) atoms, whereas in structure **19'** the molecular plane of ethylene deviates only slightly from this plane. The energies of structures **19** and **19'** are 3.2 and 3.4 kcal mol^{-1}, respectively.

Structures **19** and **19'** can be transformed into **7** and **7'**, respectively, by rotating about the Zr—C(1) bond. The transformation pathways pass through the local maxima corresponding to structures **20** and **20'** (see Scheme 3) with energies of 5.0 and 5.5 kcal mol^{-1}, respectively, and through the local minima corresponding to the above-mentioned structures **17** and **17'** (see Scheme 2) with energies of 4.4 and 5.4 kcal mol^{-1}, respectively, relative to the energy of complex **5**. Structures **20** and **20'** appear at intermediate angles of rotation about the Zr—C(1) bond. Thus, our study of the PES of the $[Cp_2ZrC_2H_5]^+ + C_2H_4$ system showed that structure **18** (**18'**) has the highest energy on the pathway **5** → **7**(**7'**). The **5** → **18'** → **19'** → **20'** → **17'** → **7'** → **6** → **9** reaction channel associated with overcoming the highest energy barrier (7.3 kcal mol^{-1}, TS **18'**) appears to be more energetically favorable. At the same time, the **5** → **18** → **19** → **20** → **17** → **7** → **6** → **9** reaction channel associated with overcoming an energy barrier of 7.3 kcal mol^{-1} (TS **18**) is characterized by the lower maximum ΔG_{298} value on the reaction pathway (Table 4). Nevertheless, the energy and thermodynamic characteristics of both reaction channels are close, so none of them can be excluded from consideration.

Table 4. Energies and standard thermodynamic characteristics of transition states for different channels of chain propagation reaction

Channel	ν_{imag} /cm^{-1}	E^*	ΔH_0^*	ΔH_{298}	ΔG_{298}	ΔS_{298}
		/kcal mol^{-1}				/cal mol^{-1} K^{-1}
			Calculations**			
4→**7**	101i	3.36	0.88	1.39	0.08	4.4
5→**12**	245i	6.78	7.13	6.63	7.78	−3.9
			This work			
4→**7**	173i	5.20	3.86	3.98	3.66	1.1
4→**7'**	173i	5.40	4.10	4.23	3.91	1.1
5→**18**	179i	7.72	6.77	7.04	5.54	5.0
5→**18'**	176i	7.30	6.40	6.64	5.73	3.0
5→**12**	268i	5.61	6.68	5.86	7.82	−6.6

* The E and ΔH_0 values in this Table correspond to the ΔH_{elec} and $\Delta H_{elec} + \Delta H_0$ values given in Ref. 9.
** Data taken from Ref. 9.

Ethylene insertion **7** → **9**

After the system has overcome the energy barriers corresponding to TS **7** and **7'**, respectively, the cleavage of the Zr—C(1) bond and the formation of the C(1)—C(3) bond occur in the coordination sphere of the zirconium ion, resulting in propagation of the polymer chain and in the formation of primary γ-agostic product $[Cp_2ZrC_4H_9]^+$ (**9**). Structure **9** is presented in Fig. 4 and the corresponding energy and geometric parameters are listed in Table 2.

Different estimates of the height of the activation barrier to ethylene insertion have been reported. Ac-

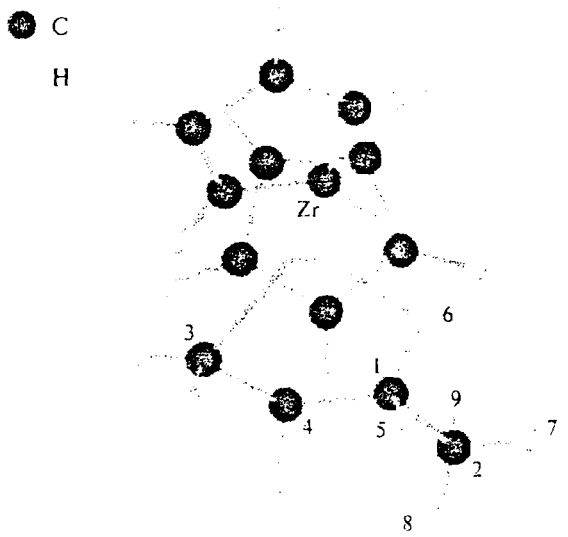

Fig. 4. Structure of primary product of ethylene insertion into the Zr—Alk bond (**9**).

cording to DFT calculations,[10] this barrier is no higher than 0.4 kcal mol^{-1}. At the same time, the barrier height estimates obtained at the RMP2—RMP4 levels of theory[4] are 7 to 10 kcal mol^{-1}. Experimental data[19—22] indicate that the activation energy of chain propagation does not exceed 7.6 kcal mol^{-1}. As was mentioned above, the **7** → **9** insertion is likely not the rate-limiting stage; hence, the activation energy of ethylene insertion should be appreciably lower than 7.6 kcal mol^{-1}.

It should also be noted that, though the ethylene insertion is preceded by the formation of an α-agostic bond, we failed to locate a local minimum corresponding to an α-agostic complex on the PES of the system under study. This is likely due to barrierless transformation of the α-agostic complex into the insertion product **9**. Previously,[8] the structure and energy of this complex were obtained by point-by-point scanning of the dependence of the energy of the system on its geometric parameters.

Ethylene insertion 5 → 13

We also considered the possibility for "direct" insertion of the ethylene molecule into complex **5**, resulting in δ-agostic product **13**. To this end, we optimized the geometry of TS **12**. The energies and thermodynamic characteristics of TS **12** are listed in Table 4. As can be seen, the energy characteristics (ΔH_0) of TS **12** and **18** are close, but the change in the entropy of the system during the reaction makes the **5** → **13** reaction pathway much less favorable than the **5** → **9** pathway. It should be noted that both of them are much less favorable than the **4** → **9** reaction pathway considered above.

Limiting stage of chain propagation

Structures **7** and **7′** have the highest energies on the **4** → **9** pathway of the chain propagation reaction, which begins with the addition of an ethylene molecule to active catalytic species **2** and results in the formation of the insertion product. Because of this, structures **7** and **7′** can be considered as common TS of the chain propagation reaction. If adduct **5** is taken as the initial compound, structures **18** (**18′**) or **12** should be considered as transition states. Since (i) the energies of TS **7** and TS **18** (**18′**, **12**) differ appreciably and (ii) interconversion of complexes **4** and **5** by means of dissociation followed by ethylene addition occurs rapidly, which is likely due to the negative ΔG of dissociation, the **4** → **7**(**7′**) → **9** sequence of transformations seems to be the most realistic to describe the chain propagation mechanism. This is in agreement with the reported results.[8]

* * *

Thus, the results of this study extend our knowledge of the mechanism of ethylene polymerization reactions by zirconocene catalysts.

Stationary points corresponding to the intermediates and TS of the reaction were located on the PES of the $[Cp_2ZrC_2H_5]^+ + C_2H_4$ system. Three different mechanisms involving the formation of β-agostic complexes **4** and **5** were considered. The corresponding activation energies differ insignificantly and lie in the range 3.9—6.8 kcal mol^{-1}.

Our calculations confirmed the previously drawn conclusion[8] that the **4** → **7**(**7′**) → **9** transformation should be considered as the rate-determining stage of the reaction. Despite this fact, the energies and thermodynamic parameters obtained in this work are in much better agreement with experimental data. For instance, the measured activation energy of chain propagation varies between 6.0 and 7.6 kcal mol^{-1}.[15—18] Previously,[8] this value (ΔH_0) was estimated at ~0.9 kcal mol^{-1},[8] whereas our calculations give 3.9 kcal mol^{-1} or higher.

Important results obtained in this work also include location of two TS, **7** and **7′**, with different geometries and energies, as well as investigation of an alternative reaction mechanism involving transformation of complex **5** into reaction product **9**.

The results obtained in this work showed that the use of the PBE density functional and extended basis sets makes it possible to improve the agreement between calculated and experimental data compared to the known methods used in the framework of the DFT computational scheme.

The authors express their gratitude to Prof. Yu. A. Ustynyuk and A. Yu. Ermilov for helpful discussions.

This work was financially supported by the Young Investigators Support Program of the President of the Russian Federation (Project No. 96-15-969997).

References

1. H. H. Brintzinger, D. Fisher, R. Mulhaupt, B. Rieger, and R. M. Waymouth, *Angew. Chem., Int. Ed. Engl.*, 1995, **34**, 1143.
2. M. Bochmannn, *J. Chem. Soc., Dalton Trans.*, 1996, 255.
3. W. Kaminsky, *J. Chem. Soc., Dalton Trans.*, 1998, 1413.
4. T. Yoshida, N. Koga, and K. Morokuma, *Organometallics*, 1995, **14**, 746.
5. T. Ziegler, *Chem. Rev.*, 1991, **91**, 651.
6. P. Margl, L. Deng, and T. Ziegler, *Organometallics*, 1998, **17**, 933.
7. P. Margl, J. C. W. Lohrenz, T. Ziegler, and P. Blöchl, *J. Am. Chem. Soc.*, 1996, **118**, 4434.
8. J. C. W. Lohrenz, T. K. Woo, and T. Ziegler, *J. Am. Chem. Soc.*, 1995, **117**, 12793.
9. T. K. Woo, L. Fan, and T. Ziegler, *Organometallics*, 1994, **13**, 2252.
10. J. C. W. Lohrenz, T. K. Woo, L. Fan, and T. Ziegler, *J. Organomet. Chem.*, 1995, **497**, 91.
11. G. L. Soloveichik, *Metalloorg. Khim.*, 1988, **1**, 277 [*Organomet. Chem. USSR*, 1988, **1** (Engl. Transl.)].
12. D. N. Laikov, *Chem. Phys. Lett.*, 1997, **281**, 151.
13. J. P. Perdew, K. Burke, and M. Ernzerhof, *Phys. Rev. Lett.*, 1996, **77**, 3865.
14. S. H. Vosko, L. Wilk, and M. Nusair, *Can. J. Phys.*, 1980, **58**, 1200.
15. A. D. Becke, *Phys. Rev.*, 1988, **A38**, 3098.
16. J. P. Perdew, *Phys. Rev.*, 1986, **B33**, 8822.
17. J. P. Perdew, *Phys. Rev.*, 1986, **B34**, 7406.
18. L. Yu. Ustynyuk, Yu. A. Ustynyuk, D. N. Laikov, and V. V. Lunin, *Izv. Akad. Nauk, Ser. Khim.*, 1999, 2248 [*Russ. Chem. Bull.*, 1999, **48**, 2222 (Engl. Transl.)].
19. J. C. W. Chien and A. Razavi, *J. Polym. Sci., Part A: Polym. Chem.*, 1988, **26**, 2369.
20. J. C. W. Chien and B.-P. Wang, *J. Polym. Sci., Part A: Polym. Chem.*, 1990, **28**, 15.
21. J. C. W. Chien, W.-M. Tasai, and M. D. Rausch, *J. Am. Chem. Soc.*, 1991, **113**, 8570.
22. J. C. W. Chien and R. Sugimoto, *J. Polym. Sci., Part A: Polym. Chem.*, 1991, **29**, 459.

Received October 4, 1999;
in revised form February 22, 2000